Atmospheric Chemistry of Two Biodiesel Model Compounds: Methyl Propionate and Ethyl Acetate

ARTICLE *in* THE JOURNAL OF PHYSICAL CHEMISTRY A · AUGUST 2011

Impact Factor: 2.69 · DOI: 10.1021/jp204819d · Source: PubMed

7 AUTHORS, INCLUDING:

Tesfaye Berhanu
Universität Bern
8 PUBLICATIONS **38** CITATIONS
SEE PROFILE

Solvejg Jørgensen
University of Copenhagen
42 PUBLICATIONS **588** CITATIONS
SEE PROFILE

Ole John Nielsen
University of Copenhagen
263 PUBLICATIONS **4,915** CITATIONS
SEE PROFILE

Matthew S Johnson
University of Copenhagen
138 PUBLICATIONS **1,686** CITATIONS
SEE PROFILE

THE JOURNAL OF PHYSICAL CHEMISTRY A

Article

pubs.acs.org/JPCA

Atmospheric Chemistry of Ethyl Propionate

Vibeke F. Andersen, Kristian B. Ørnsø, Solvejg Jørgensen, Ole John Nielsen, and Matthew S. Johnson*

Copenhagen Center for Atmospheric Research (CCAR), Department of Chemistry, University of Copenhagen, Universitetsparken 5, 2100 København Ø, Denmark

Supporting Information

ABSTRACT: Ethyl propionate is a model for fatty acid ethyl esters used as first-generation biodiesel. The atmospheric chemistry of ethyl propionate was investigated at 980 mbar total pressure. Relative rate measurements in 980 mbar N_2 at 293 ± 0.5 K were used to determine rate constants of $k(C_2H_5C(O)OC_2H_5 + Cl) = (3.11 \pm 0.35) \times 10^{-11}$, $k(CH_3CHClC(O)OC_2H_5 + Cl) = (7.43 \pm 0.83) \times 10^{-12}$, and $k(C_2H_5C(O)OC_2H_5 + OH) = (2.14 \pm 0.21) \times 10^{-12}$ cm^3 molecule^{-1} s^{-1}. At 273−313 K, a negative Arrhenius activation energy of −3 kJ mol^{-1} is observed.. The chlorine atom-initiated oxidation of ethyl propionate in 980 mbar N_2 gave the following products (stoichiometric yields): $ClCH_2CH_2C(O)OC_2H_5$ (0.204 ± 0.031), $CH_3CHClC(O)OC_2H_5$ (0.251 ± 0.040), and $C_2H_5C(O)OCHClCH_3$ (0.481 ± 0.088). The chlorine atom-initiated oxidation of ethyl propionate in 980 mbar of N_2/O_2 (with and without NO_x) gave the following products: ethyl pyruvate ($CH_3C(O)C(O)OC_2H_5$), propionic acid ($C_2H_5C(O)OH$), formaldehyde (HCHO), and, in the presence of NO_x, PAN ($CH_3C(O)OONO_2$). The lack of acetaldehyde as a product suggests that the $CH_3CH(O)C(O)OC_2H_5$ radical favors isomerization over decomposition. From the observed product yields, we conclude that H-abstraction by chlorine atoms from ethyl propionate occurs 20.4 ± 3.1%, 25.1 ± 4.0%, and 48.1 ± 8.8% from the CH_3-, $-CH_2-$, and $-OCH_2-$ groups, respectively. The rate constant and branching ratios for the reaction between ethyl propionate and the OH radical were investigated theoretically using quantum mechanical calculations and transition state theory. The stationary points along the reaction path were optimized using the CCSD(T)-F12/VDZ-F12//BH&HLYP/aug-cc-pVTZ level of theory; this model showed that OH radicals abstract hydrogen atoms primarily from the $-OCH_2-$ group (80%).

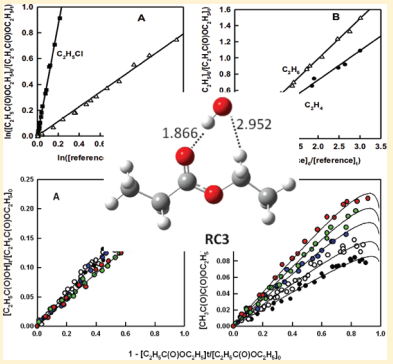

1. INTRODUCTION

The production and use of transportation biofuels has increased rapidly during the past decade due to concerns about climate change, oil price volatility, and energy security issues, combined with agricultural policy. In the U.S., the Renewable Fuel Standard established by the Energy Independence and Security Act of 2007 mandates the use of 136 billion liters of renewable fuel by 2022, which corresponds to replacement of approximately 17% of projected gasoline use for light-duty vehicles (LDVs) in 2022.[1] In Europe, the Renewable Energy Directive calls for 10% use of renewable energy in the transportation sector by 2020.[2]

In the U.S. and Brazil, the dominant biofuel is ethanol produced from corn and sugar cane, whereas fatty acid methyl esters (FAMEs) made from transesterification of plant oils or animal fats are the dominant biofuel in the EU.[3] Ethanol is typically blended into gasoline before use (e.g., in E10, E25, E85), and FAME is typically blended into petroleum diesel before use (e.g., in B2, B20). While FAMEs are cheapest to produce, alkyl esters of larger alcohols such as fatty acid ethyl esters (FAEEs) are also used as biofuels. From a renewable fuel perspective, the use of FAEEs is more desirable than the use of FAMEs since ethanol can be produced from plant material. Compared to FAMEs, fatty acid esters of longer chained alcohols have improved cold flow.[4,5] Fatty acid alkyl esters are typically categorized as "biodiesel", as distinct from hydrotreated vegetable oils which are "renewable diesel".

Production of biodiesel has been commercially important since the beginning of the 1990s. In 2010, global biodiesel production reached approximately 20 billion liters with approximately half of the production taking place in Europe, where it is produced mainly from rapeseed and sunflower. A large fraction of the remaining production takes place in the US where the main feedstock is soybeans.[3−6]

The widespread use of fatty acid alkyl esters in diesel blends will lead to their release into the atmosphere. The esters present in biodiesel (e.g., methyl oleate, methyl linoleate) have low vapor pressures and are difficult to study in smog chamber systems. In the present study, we investigate, using experimental and computational methods, the chemistry of ethyl propionate as a model for the larger esters present in biodiesel. Atmospheric degradation of ethyl propionate is initiated by photochemical oxidants. In ambient air, the most important reactive species is the hydroxyl radical, which is present at a concentration of approximately 1 × 10^6 radicals cm^{-3}.[7]

Received: January 27, 2012
Revised: April 18, 2012
Published: April 23, 2012

dx.doi.org/10.1021/jp300897t | J. Phys. Chem. A 2012, 116, 5164−5179

Table 1. Rate Constants (Units of 10^{-12} cm^3 molecule^{-1} s^{-1}) for Reactions of Chlorine Atoms and OH Radicals with Ethyl Propionate[a]

reaction		k	method	temp (K)	ref
$C_2H_5C(O)OC_2H_5$ + Cl → products	(1)	33.1 ± 3.7	RR	273	this study
		31.1 ± 3.5	RR	293	this study
		27.6 ± 3.7	RR	313	this study
		37 ± 1	RR	296	Cometto et al., 2009[14]
$CH_3CHClC(O)OC_2H_5$ + Cl → products	(2)	7.43 ± 0.83	RR	293	this study
$C_2H_5C(O)OC_2H_5$ + OH → products	(3)	2.14 ± 0.21	RR	293	this study
		6.76	CCSD(T)-F12/VDZ-F12//BH&HLYP/aug-cc-pVTZ	298	this study
		2.14 ± 0.30	FP-RF	296	Wallington et al., 1988[15]
		2.1 ± 0.2	PLP-LIF	298	Cometto et al., 2009[14]
		2.4 ± 0.1	RR	298	Cometto et al., 2009[14]

[a]RR: relative rate; FP-RF: flash photolysis resonance fluorescence; PLP-LIF: pulsed laser photolysis−laser induced fluorescence.

Another key atmospheric oxidant is the chlorine atom. The most important source of this compound is photolysis of chlorine-containing species generated in sea salt aerosols.[8] In polluted areas, surface reactions of gaseous hydrogen chloride and nitrogen oxides can lead to the production of ClNO and $ClNO_2$, which can photolyze to produce chlorine atoms.[9] Reaction mechanisms involving Cl are similar to those of the OH-radical, with rate constants 10−100 times larger than those for the corresponding OH-reactions. It is therefore convenient to use Cl-atom reactions as models for OH-radical reactions. In the atmosphere, oxidation by Cl atoms may be important in the marine boundary layer where peak concentrations have been observed to be 10^3−10^6 radicals cm^{-3}.[10]

Detailed kinetic and mechanistic data concerning these reactions are needed as inputs for atmospheric chemistry models to assess the environmental impacts associated with release of esters into the air. The available database concerning the atmospheric chemistry of esters is limited,[11,12,13] and the present work was undertaken to improve our understanding of the chemistry of this class of oxygenated organic compounds.

In a previous study we determined the atmospheric oxidation mechanisms of the two $C_4H_8O_2$ isomers methyl propionate and ethyl acetate.[13] The study showed that the ethyl ester has a higher reactivity toward OH radicals than the methyl ester. Furthermore, while the reaction of ethyl acetate with Cl occurred exclusively on the alkoxy end of the molecule, both the acyl end and the alkoxy end of methyl propionate showed reactivity toward Cl.[13] In the present study we have investigated the reactivities of esters related to their structure in greater detail by determining the relative reactivities of the alkoxy and the acyl ends of an ester containing both a propionate and an ethyl group. We conducted an experimental investigation of the kinetics and products of the OH radical and chlorine atom-initiated oxidation of ethyl propionate at 980 mbar of N_2/O_2 diluent with and without added NO at 293 ± 0.5 K. The Arrhenius activation energy for the Cl-initiated oxidation was determined in the temperature interval 273−313 K, and we conducted a computational study of the kinetics of reactions of OH radicals with ethyl propionate.

The present study complements our recent study of the atmospheric chemistry of methyl propionate and ethyl acetate, and it adds to the understanding of the differences in reactivity of methyl and ethyl esters.

One previous study of k(ethyl propionate + Cl)[14] and two studies of k(ethyl propionate + OH)[14,15] have been reported. Results from the previous studies are listed in Table 1. There are no previous determinations of k(ethyl-2-chloropropionate + Cl). To the best of our knowledge, this is the first study of the Cl-initiated oxidation mechanism of ethyl propionate.

2. EXPERIMENTAL SETUP

Experiments were performed in the photochemical reactor at the Copenhagen Center for Atmospheric Research (CCAR). The system has been described in detail elsewhere[16] and is summarized here. The system consists of a 100-L quartz reaction chamber sealed at both ends with stainless steel flanges and surrounded by 8 UV-A (325−380 nm), 16 UV-C (254 nm), and 12 broadband sun lamps. The system is enclosed in an insulating box equipped with a temperature control system to ensure stable (within 0.5 K) temperatures during experiments. Gas mixtures in the chamber were monitored with a Bruker IFS 66v/s FTIR spectrometer using an IR path length of 64 m and a resolution of 0.13 cm^{-1}. In addition, samples from product studies were collected on Tenax tubes for gas chromatography−mass spectrometry (GC-MS) analysis with an Agilent 6850 GC connected to an Agilent 5975C VL MS with an HED-EM triple axis mass selective detector. In the present study, a HP-5MS 5% phenyl and 95% polysiloxane capillary column of 50 m × 200 μm with a phase thickness of 0.33 μm was used. The oven program was set to a 21 min cycle with an initial temperature of 40 °C for 3 min after which time the oven was heated to 180 °C at a rate of 10 °C min^{-1} and kept at 180 °C for 5 min.

3. MATERIALS AND METHOD

Rate constants for the following reactions were determined:

$$C_2H_5C(O)OC_2H_5 + Cl \rightarrow \text{products} \quad (1)$$

$$CH_3CHClC(O)OC_2H_5 + Cl \rightarrow \text{products} \quad (2)$$

$$C_2H_5C(O)OC_2H_5 + OH \rightarrow \text{products} \quad (3)$$

The rate constant for reaction 1 was determined at 273, 293, and 313 K, and the rate constants for reactions 2 and 3 were determined at 293 K.

The reaction rates were determined using the relative rate method. Assuming that the reactant and reference compounds are only lost via the reaction of interest and that neither the reactant nor the reference is formed in the system the following relation is valid:

dx.doi.org/10.1021/jp300897t | J. Phys. Chem. A 2012, 116, 5164−5179

Table 2. Reference Rate Constants Used in This Work

reaction		temp (K)	rate constant (cm^3 $molecule^{-1}$ s^{-1})	ref
$C_2H_5Cl + Cl \rightarrow$ products	(4)	273	$(7.51 \pm 0.76) \times 10^{-12}$	Wine and Semmes, 1983[39]
$C_2H_5Cl + Cl \rightarrow$ products	(4)	293	$(8.04 \pm 0.57) \times 10^{-12}$	Wine and Semmes, 1983[39]
$C_2H_5Cl + Cl \rightarrow$ products	(4)	313	$(8.68 \pm 1.62) \times 10^{-12}$	Wine & Semmes, 1983[39]
$C_2H_4 + Cl \rightarrow$ products	(5)	293	$(9.29 \pm 0.51) \times 10^{-11}$	Wallington et al., 1990[40]
$C_2H_6 + Cl \rightarrow$ products	(6)	273	$(5.75 \pm 0.36) \times 10^{-11}$	Atkinson et al., 2006[41]
$C_2H_6 + Cl \rightarrow$ products	(6)	293	$(5.90 \pm 0.37) \times 10^{-11}$	Atkinson et al., 2006[41]
$C_2H_6 + Cl \rightarrow$ products	(6)	313	$(6.03 \pm 0.37) \times 10^{-11}$	Atkinson et al., 2006[41]
$c\text{-}C_6H_{12} + OH \rightarrow$ products	(7)	293	$(6.37 \pm 0.30) \times 10^{-12}$	Calvert et al., 2008[42]
$C_3H_8 + OH \rightarrow$ products	(8)	293	$(1.10 \pm 0.09) \times 10^{-12}$	Atkinson et al., 2006[41]

$$\ln\left(\frac{[\text{reactant}]_0}{[\text{reactant}]_t}\right) = \frac{k_{\text{reactant}}}{k_{\text{reference}}} \ln\left(\frac{[\text{reference}]_0}{[\text{reference}]_t}\right) \quad \text{(I)}$$

where $[\text{reactant}]_0$ and $[\text{reference}]_0$ are the initial concentrations of reactant and reference, respectively, and $[\text{reactant}]_t$ and $[\text{reference}]_t$ are the concentrations of reactant and reference at time t. Plotting the loss of reactant versus reference compound gives a straight line with slope $k_{\text{reactant}}/k_{\text{reference}}$. Unless stated, all quoted uncertainties are two standard deviations resulting from least-squares regressions and include uncertainties in the analysis of the IR spectra (typically 5−10%).

Reactions 4−8 were employed as the reference reactions. The reference rate constants used are listed in Table 2.

$$C_2H_5Cl + Cl \rightarrow \text{products} \quad (4)$$

$$C_2H_4 + Cl \rightarrow \text{products} \quad (5)$$

$$C_2H_6 + Cl \rightarrow \text{products} \quad (6)$$

$$c\text{-}C_6H_{12} + OH \rightarrow \text{products} \quad (7)$$

$$C_3H_8 + OH \rightarrow \text{products} \quad (8)$$

k_1 was determined relative to k_4, k_5, and k_6, k_2 was determined relative to k_4 and k_6, and k_3 was determined relative to k_7 and k_8. All chemicals were obtained from commercial sources: $C_2H_5C(O)OC_2H_5$ (99%, Aldrich), $CH_3CHClC(O)OC_2H_5$ (97%, Aldrich), C_2H_5Cl (99.7%, Gerling Holz + CO), C_2H_6 (99.95%, Fluka), C_2H_4 (99.5%, Aldrich), $c\text{-}C_6H_{12}$ (99.5%, Aldrich), and C_3H_8 (98%, Aldrich).

Atomic chlorine was produced by photolysis of Cl gas (reaction 9) with UV-A light, and OH was generated by photolysis of ozone with UV-C light followed by reaction with water vapor (reactions 10 and 11).

$$Cl_2 + h\nu \rightarrow 2Cl \quad (9)$$

$$O_3 + h\nu \rightarrow O_2 + O(^1D) \quad (10)$$

$$O(^1D) + H_2O \rightarrow 2OH \quad (11)$$

O_3 was generated from O_2 with an ozone generator from O_3 Technology (model AC-20), and condensed on silica gel that was cooled with ethanol and dry ice to approximately −70 °C.

Relative rate experiments were performed in 980 mbar of N_2 diluent in the presence of ethyl propionate, one reference, and oxidant. In the experiments with Cl, the initial concentrations of reactants were 7−13 ppm, and the initial concentrations of references were 12−25 ppm. For experiments with OH, the initial concentrations of ethyl propionate and reference were 13−31 ppm each. The initial concentration of ozone and water vapor or Cl_2 was approximately 5 times the total concentration of reactants. Product studies were performed in 980 mbar of N_2/O_2 diluent with O_2 partial pressures of 0−980 mbar in the presence and absence of NO. Experiments in the presence of NO were performed with NO concentrations of 34−56 ppm. Product and reactant reference spectra were recorded by introducing a known amount of reference compound into the chamber and recording a spectrum. Photolysis intervals were typically between 5 s and 10 min, and an IR spectrum was recorded after each photolysis step. In the product studies, samples were collected on Tenax tubes for GC-MS analysis after each photolysis step.

4. COMPUTATIONAL DETAILS

In previous work we computed the energetics of the reaction path for methyl acetate reacting with the hydroxyl radical. The same method of computing the energetics was used in the present study. The geometries of the species in this study were optimized using density functional theory, BH&HLYP[17,18]/aug-cc-pVTZ.[19] The calculated frequencies were used to characterize the stationary points (a minimum or a saddle point) and to estimate the zero point vibrational energy (ZPE). The BH&HLYP/aug-cc-pVTZ calculations were performed using Gaussian 03.[20] Spin contamination is not considered to be severe since the expectation value of the total spin was less than 0.78 before and 0.75 after spin annihilation.

The energies are refined using an explicitly correlated CCSD(T)-F12a[21] method with the VDZ-F12[22] basis set. These calculations were performed using the MOLPRO 2010.1 package.[23] Values of the T1 and D1 diagnostics range between 0.012 and 0.023 and 0.05−0.14, respectively. This indicates that the CCSD(T)-F12a energies are reliable.

We assume that the reaction between ethyl propionate and the hydroxyl radical proceeds via a two-step mechanism. The first step involves a fast pre-equilibrium (K_{eq}) between the reactants and the reaction complex and the second step is the hydrogen abstraction with the rate constant k_2. The overall rate constant is where the equilibrium constant (K_{eq}) and rate constant (k_2) are given by

$$K_{eq} = \sigma_{eq}\left(\frac{Q_{RC}}{Q_{R1}Q_{R2}}\right)\exp\left(-\frac{E_{RC} - E_{R1} - E_{R2}}{k_bT}\right) \quad \text{(II)}$$

dx.doi.org/10.1021/jp300897t | J. Phys. Chem. A 2012, 116, 5164−5179

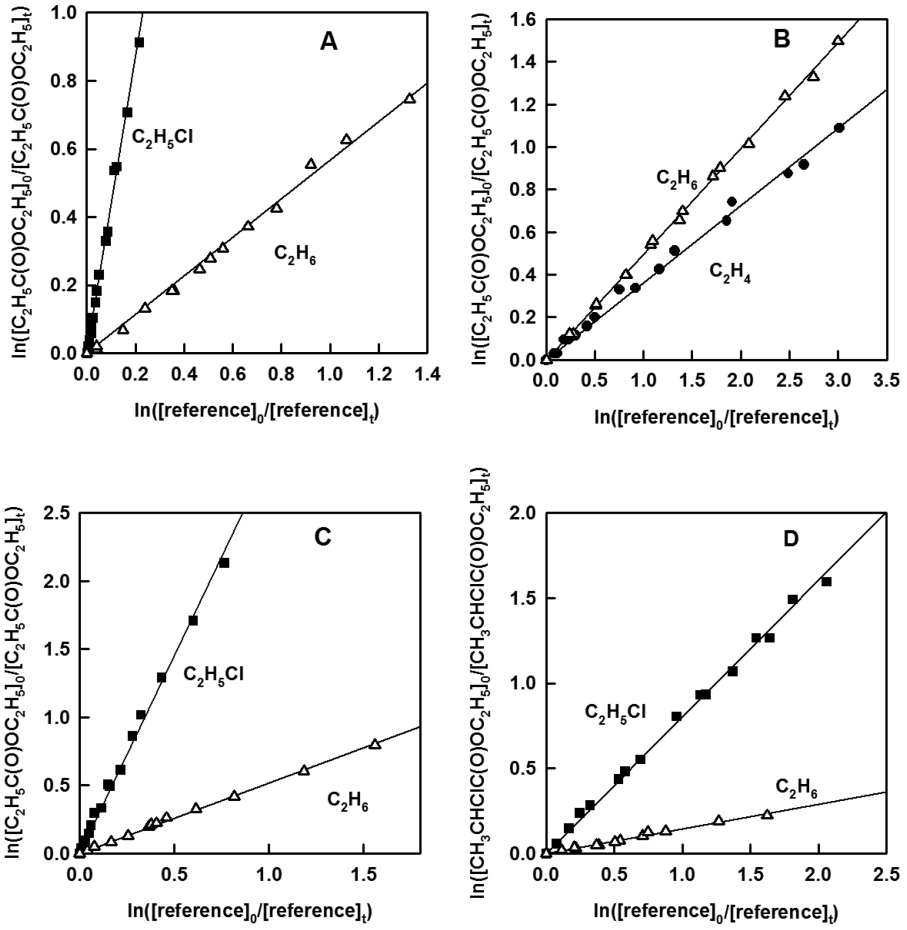

Figure 1. Relative rate plots for the reaction of ethyl propionate (Panels A-C) and ethyl-2-chloropropionate (Panel D) with Cl in 980 mbar N_2 at 273 ± 0.5 K (Panel A), 293 ± 0.5 K (Panels B and D) and 313 ± 0.5 K (Panel C).

$$k = \sigma\kappa(T)\frac{k_b T}{h}\left(\frac{Q_{TS}}{Q_{RC}}\right)\exp\left(-\frac{E_{TS} - E_{RC}}{k_b T}\right) \quad \text{(III)}$$

where σ is the symmetry factor, i.e., the number of identical reaction paths; k_b is Boltzmann's constant; h is Planck's constant; T is the temperature; Q is the total partition function; and finally, E is the energy at 0 K. The quantum tunnelling effect is estimated using an asymmetric Eckart potential.[24]

5. RELATIVE RATE RESULTS

To test for photolysis, mixtures containing ethyl propionate and one reference compound (but not Cl_2 or O_3/H_2O) in N_2 were irradiated using conditions (number of lamps and time span) similar to those used in the relative rate experiments. To test for unwanted heterogeneous reactions, mixtures (including Cl_2 or O_3/H_2O) were left for 10−30 min in the chamber in the dark. There was no discernible loss (<1%) of the reactants in these control experiments.

5.1. Cl Experiments. C_2H_5Cl, C_2H_4, and C_2H_6 were used as reference compounds to study the reaction of chlorine atoms with ethyl propionate and ethyl-2-chloropropionate. Ethyl propionate was monitored using the C−O stretching vibration absorbing in the range 1150−1260 cm^{-1}. The absorption peak due to C═O stretching in the range of 1720−1800 cm^{-1} was used to follow ethyl-2-chloropropionate, and C_2H_5Cl was monitored using its absorption peak at 1289 cm^{-1}. The absorption overtone peak at 1889 cm^{-1} from the C−H bend was used for C_2H_4, and the absorption peak from the C−H stretching vibration at 2895 cm^{-1} was used to monitor C_2H_6. Relative rate plots are shown in Figure 1. Linear least-squares analyses of the data in Figure 1 together with resultant rate constants are provided in Table 3. In all cases, the rate constants obtained relative to the two reference reactions agree to within the error limits. We determine the following final room temperature (293 ± 0.5 K) values, which are the average of the individual determinations with error limits from the weighted average of the determinations:

Table 3. Results for Relative Rate Studies of the Cl- and OH-Initiated Oxidations of Ethyl Propionate and Ethyl-2-chloropropionate

reaction	temp (K)	$k_{ester}/k_{reference}$	rate constant (10^{11} cm^3 $molecule^{-1}$ s^{-1})
(1) relative to (4)	273	4.354 ± 0.564	3.27 ± 0.54
(1) relative to (6)	273	0.580 ± 0.089	3.34 ± 0.51
(1) relative to (5)	293	0.354 ± 0.051	3.29 ± 0.47
(1) relative to (6)	293	0.496 ± 0.057	2.93 ± 0.53
(1) relative to (4)	313	2.824 ± 0.421	2.45 ± 0.59
(1) relative to (6)	313	0.509 ± 0.067	3.07 ± 0.45
(2) relative to (4)	293	0.790 ± 0.102	0.635 ± 0.094
(2) relative to (6)	293	0.144 ± 0.022	0.850 ± 0.140
(3) relative to (7)	293	0.332 ± 0.044	0.211 ± 0.030
(3) relative to (8)	293	1.97 ± 0.24	0.217 ± 0.032

dx.doi.org/10.1021/jp300897t | J. Phys. Chem. A 2012, 116, 5164−5179

$$k_1 = (3.11 \pm 0.35) \times 10^{-11}\ \text{cm}^3\ \text{molecule}^{-1}\ \text{s}^{-1}$$

$$k_2 = (7.43 \pm 0.83) \times 10^{-12}\ \text{cm}^3\ \text{molecule}^{-1}\ \text{s}^{-1}$$

The small negative temperature dependence observed for reaction 1 (see Table 1) corresponds to an Arrhenius activation energy of about −3 kJ mol^{-1}.

The negative activation energy suggests the formation of a prereaction complex that will have a higher tendency to undergo unimolecular decomposition back to its parent compounds ($C_2H_5C(O)OC_2H_5$ and Cl) at higher temperatures. A similar result has been observed by Cuevas et al.[25] for the reaction of Cl with ethyl acetate.

As seen from Table 1, the room-temperature rate constant for reaction 1 is significantly different from the previous determination by Cometto et al.[14] The reason for this discrepancy is probably due to an underestimation of the error bar in the previous study (the error is 2.7% and does not include experimental errors).

The present study provides the first determination of the rate constant, k_2, for the reaction between ethyl-2-chloropropionate and chlorine atoms.

5.2. OH Experiments. *c*-C_6H_{12} and C_3H_8 were used as reference compounds in the study of the reaction of OH radicals with ethyl propionate. *c*-C_6H_{12} and C_3H_8 were monitored using the absorption peaks from the C−H stretching vibrations at 2830−2890 and 2968 cm^{-1}, respectively. Relative rate plots are shown in Figure 2. Linear least-squares analyses of the data in Figure 2 together with resultant rate constants are provided in Table 3. The rate constants obtained relative to the two reference reactions agree to within the error limits. We cite the following final room temperature value which is the average of the individual determinations with error limits from the weighted average of the determinations:

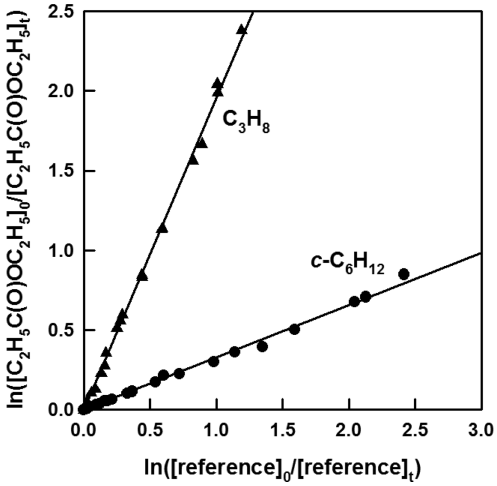

Figure 2. Relative rate plots for the reaction of ethyl propionate with OH in 980 mbar N_2 at 293 ± 0.5 K.

$$k_3 = (2.14 \pm 0.21) \times 10^{-12}\ \text{cm}^3\ \text{molecule}^{-1}\ \text{s}^{-1}$$

The rate constant determined in the present study is in excellent agreement with the one determined by Wallington et al.,[15] and it is in good agreement with both determinations by Cometto et al.[14]

The rate constant is also in good agreement with that predicted by structure activity calculations performed with EPA's AOPWin calculator. According to these calculations, k_3 = 2.12 × 10^{-12} cm^3 molecule^{-1} s^{-1}.[26]

6. RESULTS OF THE Cl-INITIATED PRODUCT STUDY

6.1. Results in 980 mbar N_2. Cl atoms initiate oxidation of ethyl propionate by H-abstraction via reactions 1a−1d.

$$C_2H_5C(O)OC_2H_5 + Cl \rightarrow {}^{\bullet}CH_2CH_2C(O)OC_2H_5 + HCl \quad (1a)$$

$$C_2H_5C(O)OC_2H_5 + Cl \rightarrow CH_3C^{\bullet}HC(O)OC_2H_5 + HCl \quad (1b)$$

$$C_2H_5C(O)OC_2H_5 + Cl \rightarrow C_2H_5C(O)OC^{\bullet}HCH_3 + HCl \quad (1c)$$

$$C_2H_5C(O)OC_2H_5 + Cl \rightarrow C_2H_5C(O)OCH_2CH_2^{\bullet} + HCl \quad (1d)$$

In the absence of oxygen, the reaction of the radicals produced by reactions 1a−1d can react with Cl_2 to produce monochlorinated compounds as illustrated by reaction 12 for the radical produced in reaction 1a.

$${}^{\bullet}CH_2CH_2C(O)OC_2H_5 + Cl_2 \rightarrow ClCH_2CH_2C(O)OC_2H_5 + Cl \quad (12)$$

This monochlorinated compound, as well as ethyl-2-chloropropionate ($CH_2CHClC(O)OC_2H_5$), were identified both in the Fourier transform infrared (FTIR) and in the GC-MS analysis, evidencing H-abstraction by Cl from the acyl end of the molecule. In addition, peaks in the FTIR spectrum at 1103, 1156, 1282, and 1755−1845 cm^{-1} and a peak in the chromatogram with retention time of 11.3 min and mass peaks of m/z = 57, 63, and 101 are likely to be due to the formation of 1-chloroethyl propionate ($C_2H_5C(O)OCHClCH_3$). This assumption is based on comparison of the IR spectrum with a calculated spectrum of this compound. In Figure 3, the relative increases in the three products are plotted versus the relative decrease in ethyl propionate. The concentration of 1-chloroethyl propionate has been estimated from the absorbance of the C═O peak at 1755−1845 cm^{-1}. The yields of 1-chloroethyl propionate and ethyl-3-chloropropionate correlate linearly with the loss of ethyl propionate. From the slopes of the linear plots, we conclude that H-abstraction by Cl atoms from ethyl propionate occurs 20.4 ± 3.1% from the β-carbon atom (reaction 1a) and 48.1 ± 8.8% from the secondary carbon on the ethyl end of the molecule (reaction 1c). Quoted errors correspond to two standard deviations from the fits and additional 10% experimental error.

The decrease in the yield of ethyl-2-chloropropionate at high (>70%) consumption of ethyl propionate reflects the loss of ethyl-2-chloropropionate via reaction with Cl atoms. The shape of the plot provides information of both the yield of this product from ethyl propionate and of the reactivity of the product with Cl atoms. The equation of Meagher et al.[27] has been fitted to the data:

dx.doi.org/10.1021/jp300897t | J. Phys. Chem. A 2012, 116, 5164−5179

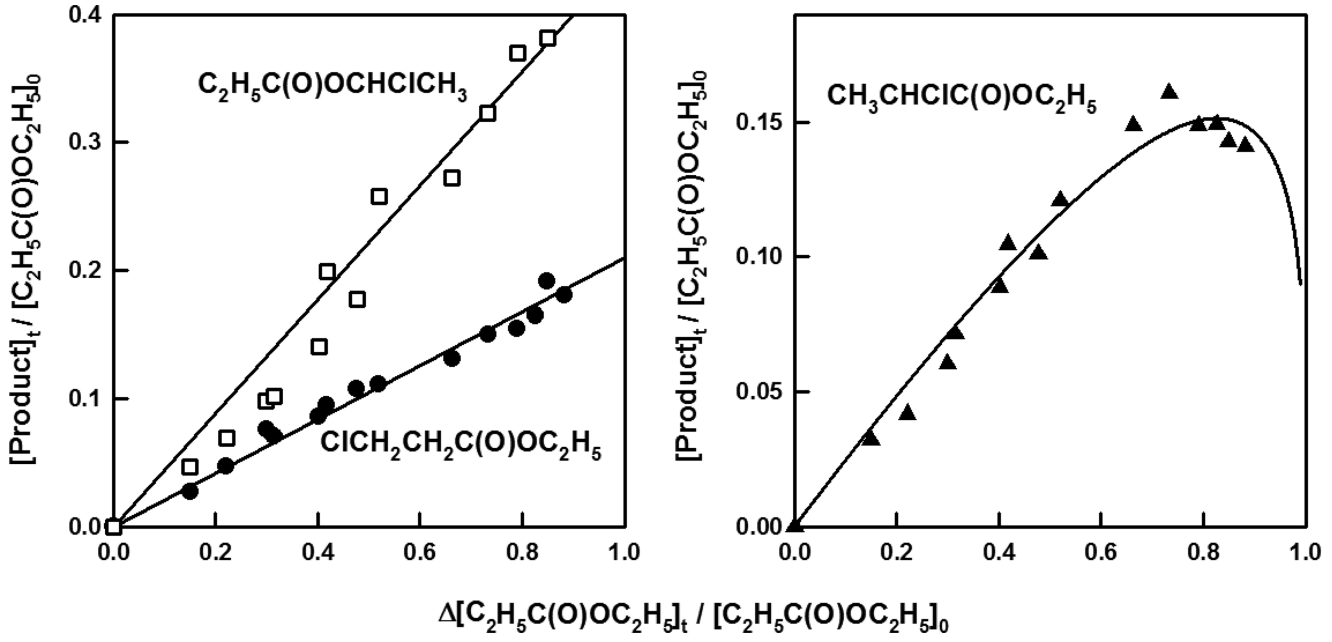

Figure 3. Formation of 1-chloroethyl propionate (squares), ethyl-3-chloropropionate (circles), and ethyl-3-chloropropionate (triangles) versus loss of ethyl propionate in 980 mbar total pressure of N_2.

Scheme 1. Suggested Reaction Mechanism of the Radical Produced by Reaction 1a[a]

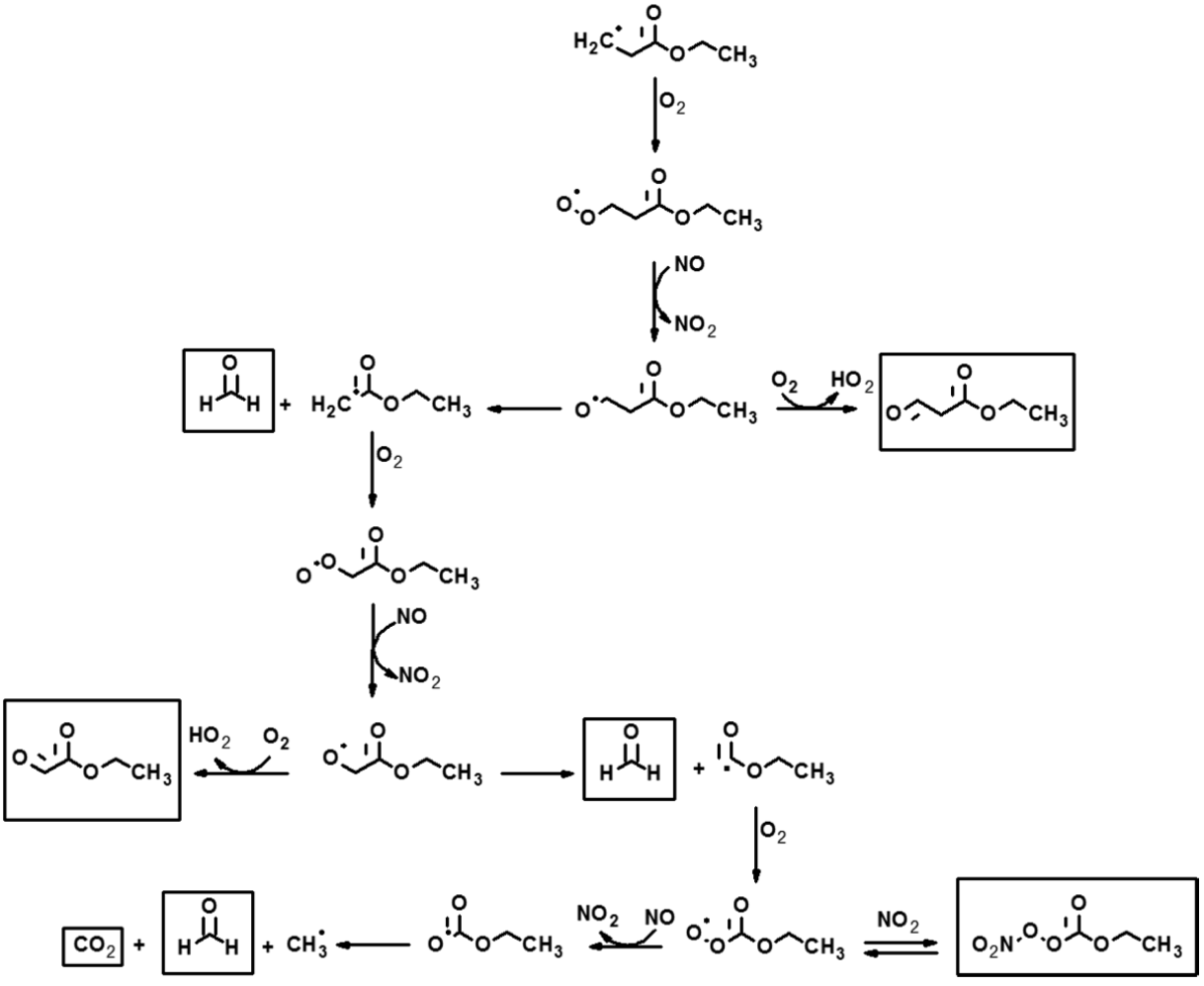

[a]Boxes indicate non radical products.

dx.doi.org/10.1021/jp300897t | J. Phys. Chem. A 2012, 116, 5164−5179

Scheme 2. Suggested Reaction Mechanism for the Radical Produced by Reaction 1b[a]

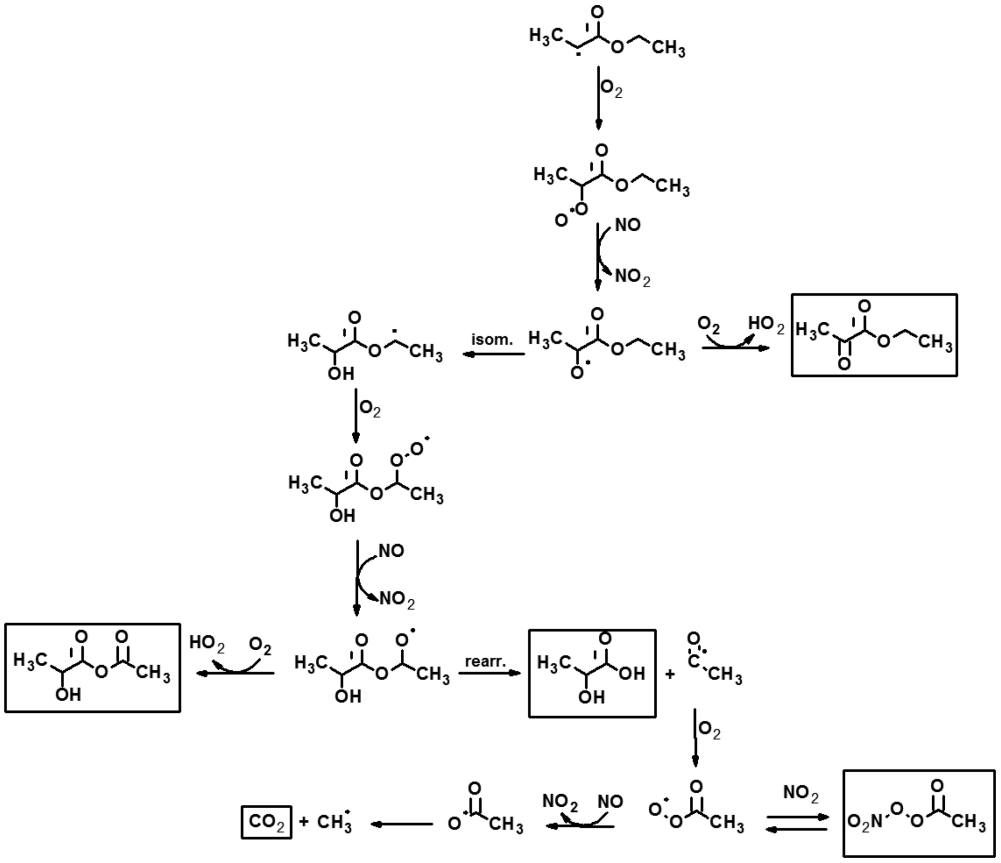

[a]Boxes indicate non-radical products.

$$\frac{[CH_3CHClC(O)OC_2H_5]_t}{[C_2H_5C(O)OC_2H_5]_{t=0}} = \frac{\alpha}{1-\frac{k_2}{k_1}}(1-x)\left[(1-x)^{(k_2/k_1)-1}-1\right] \quad \text{(IV)}$$

where α is the yield of ethyl-2-chloropropionate from the Cl initiated oxidation of ethyl propionate, k_1 and k_2 are the rate constants for reactions 1 and 2, and x is the fractional loss of ethyl propionate defined as

$$x = 1 - \frac{[C_2H_5C(O)OC_2H_5]_t}{[C_2H_5C(O)OC_2H_5]_{t=0}} \quad \text{(V)}$$

The best fit was obtained with $\alpha = 0.251 \pm 0.040$ and $k_2/k_1 = 0.289 \pm 0.105$. Quoted errors correspond to two standard deviations from the fits and additional 10% experimental error. The rate constant ratio determined from the fit is consistent with the results reported in section 5.1: $k_2/k_1 = 0.245 \pm 0.035$. From the value of α we conclude that 25.1 ± 4.0% of the reaction of ethyl propionate with Cl atoms occurs by H-abstraction from the α-carbon atom (reaction 1b).

6.2. Results in 980 mbar N_2/O_2 in the Absence of NO. The reaction mechanism of ethyl propionate was studied with oxygen partial pressures of 50, 100, 200, 500, and 980 mbar in 980 mbar total pressure of N_2 in the absence of NO.

In the presence of oxygen, the radicals generated in reactions 1a−1d will react with oxygen to form peroxy radicals. In the absence of NO, the peroxy radicals will react with other peroxy radicals to produce alkoxy radicals. The sequence is illustrated by reactions 13 and 14 for the radical generated in reaction 1a. The suggested reaction mechanism initiated by reaction 1a is shown in Scheme 1.

$$CH_2CH_2C(O)OC_2H_5 + O_2 \rightarrow OOCH_2CH_2C(O)OC_2H_5 \quad (13)$$

$$OOCH_2CH_2C(O)OC_2H_5 + RO_2 \rightarrow OCH_2CH_2C(O)OC_2H_5 + RO + O_2 \quad (14)$$

Reaction of the β-alkoxy radical with O_2 leads to the formation of $CH(O)CH_2C(O)OC_2H_5$ (reaction 15). An additional fate of the alkoxy radical is decomposition to produce formaldehyde and the $CH_2C(O)OC_2H_5$ radical (reaction 16).

$$OCH_2CH_2C(O)OC_2H_5 + O_2 \rightarrow CH(O)CH_2C(O)OC_2H_5 + HO_2 \quad (15)$$

$$OCH_2CH_2C(O)OC_2H_5 \rightarrow HCHO + CH_2C(O)OC_2H_5 \quad (16)$$

The $CH_2C(O)OC_2H_5$ will react with O_2 and RO_2 in a sequence similar to reactions 13 and 14 to produce the alkoxy radical $OCH_2C(O)OC_2H_5$ which can either react with O_2 to produce $CH(O)C(O)OC_2H_5$ or decompose to produce formaldehyde and $C(O)OC_2H_5$. The reactions are similar to reactions 15 and 16.

Neither $CH(O)CH_2C(O)OC_2H_5$ nor $CH(O)C(O)OC_2H_5$ were commercially available, and their presence could not be

dx.doi.org/10.1021/jp300897t | J. Phys. Chem. A 2012, 116, 5164−5179

confirmed in the IR spectra. A product observed in the gas chromatogram with a retention time of 14.1 min suggests the formation of $CH(O)CH_2C(O)OC_2H_5$. The corresponding mass spectrum shows peaks of m/z = 43 and 87, possibly from the $[CH(O)CH_2]^+$ and $[CH_2C(O)OC_2H_5]^+$ fragments, respectively.

A suggested reaction mechanism initiated by H-abstraction from the α-carbon atom (reaction 1b) is shown in Scheme 2. The alkoxy radical generated by reactions similar to reactions 13 and 14 from the radical generated by reaction 1b can either react with oxygen to produce ethyl pyruvate ($CH_3C(O)C(O)OC_2H_5$) (reaction 17), decompose to produce acetaldehyde and $C(O)OC_2H_5$ (reaction 18), or undergo isomerization to produce $CH_3CH(OH)C(O)OCHCH_3$ (reaction 19).

$$CH_3CH(O)C(O)OC_2H_5 + O_2 \rightarrow CH_3C(O)C(O)OC_2H_5 + HO_2 \quad (17)$$

$$CH_3CH(O)C(O)OC_2H_5 \rightarrow CH_3CHO + C(O)OC_2H_5 \quad (18)$$

$$CH_3CH(O)C(O)OC_2H_5 \rightarrow CH_3CH(OH)C(O)OCHCH_3 \quad (19)$$

Reaction 19 is a 1,5-hydrogen shift occurring through a six-membered ring.[28] The alkoxy radical generated from the $CH_3CH(OH)C(O)OCHCH_3$ radical (by reactions with O_2 and RO_2 similar to reactions 13 and 14) can either react with O_2 to produce $CH_3CH(OH)C(O)OC(O)CH_3$ (reaction 20), rearrange to produce $CH_3CH(OH)C(O)OH$ and $C(O)CH_3$ (reaction 21), or decompose to produce acetaldehyde, CO_2, and CH_3CHOH (reaction 22).

$$CH_3CH(OH)C(O)OCH(O)CH_3 + O_2 \rightarrow CH_3CH(OH)C(O)OC(O)CH_3 + HO_2 \quad (20)$$

$$CH_3CH(OH)C(O)OCH(O)CH_3 \rightarrow CH_3CH(OH)C(O)OH + C(O)CH_3 \quad (21)$$

$$CH_3CH(OH)C(O)OCH(O)CH_3 \rightarrow CH_3CHOH + CO_2 + CH_3CHO \quad (22)$$

Reaction 21 is similar to the α-ester rearrangement observed for methyl and ethyl esters,[13,29−34] occurring through a five membered ring.

Reaction 17 was confirmed by observation of ethyl pyruvate as demonstrated in Figure 4 showing spectra obtained before (panel A) and after (panel B) 85 s irradiation of a mixture of 9.5 ppm of ethyl pyruvate and 50.6 ppm of Cl_2 in 980 mbar air. Panel C shows the product spectrum after subtracting IR features from ethyl propionate from the spectrum in panel B. Comparison of this spectrum with the spectrum in panel D demonstrates the formation of propionic acid. The residual spectrum after subtraction of IR features from propionic acid from the spectrum in panel C is shown in panel E. Comparison of this spectrum with the spectrum in panel F demonstrates the formation of ethyl pyruvate. Absorption peaks from formaldehyde are also observed.

No acetaldehyde was observed in the spectra, and reaction 18 as well as reaction 22 can, therefore, be excluded. Neither $CH_3CH(OH)C(O)OC(O)CH_3$ nor $CH_3CH(OH)C(O)OH$ were commercially available, and their presence could not be

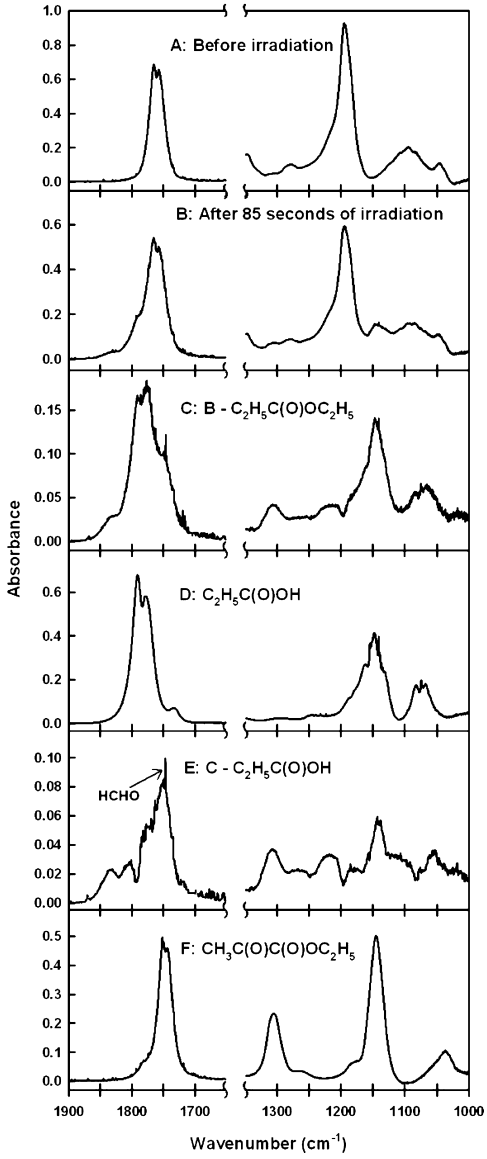

Figure 4. Spectra of a mixture of ethyl propionate and Cl_2 in air before (A) and after (B) 85 s of irradiation. The product spectrum after subtracting the spectrum in panel A from the one in panel B is shown in panel C. Comparison of this spectrum with the spectrum in panel D shows the formation of propionic acid. Panel E shows the residual spectrum after subtracting the spectrum in panel D from the one in panel C. Comparison of this spectrum with the spectrum in panel F shows the formation of ethyl pyruvate. Absorption peaks from formaldehyde (indicated by arrow in panel E) are also observed.

confirmed with FTIR analysis. The peak observed in the gas chromatogram with a retention time of 14.1 min is believed to be due to the formation of $CH(O)CH_2C(O)OC_2H_5$, although this peak may possibly be due to $CH_3CH(OH)C(O)OC(O)CH_3$ giving the two mass fragments $[C(O)CH_3]^+$ (m/z = 43) and $[C(O)OC(O)CH_3]^+$ (m/z = 87). Furthermore, a peak in the chromatogram with a retention time of 10.6 min suggests the formation of $CH_3CH(OH)C(O)OH$. The characteristic peaks in the mass spectrum with m/z = 45 and 75 can be assigned to $[C(O)OH]^+$ and $[CH(OH)C(O)OH]^+$ fragments, respectively.

The suggestion that isomerization of the $CH_3CH(O)C(O)OC_2H_5$ alkoxy radical (reaction 19) occurs rather than decomposition (reaction 18) is in contrast to what has been

dx.doi.org/10.1021/jp300897t | J. Phys. Chem. A 2012, 116, 5164−5179

Scheme 3. Suggested Reaction Mechanism for the Radical Produced by Reaction 1c[a]

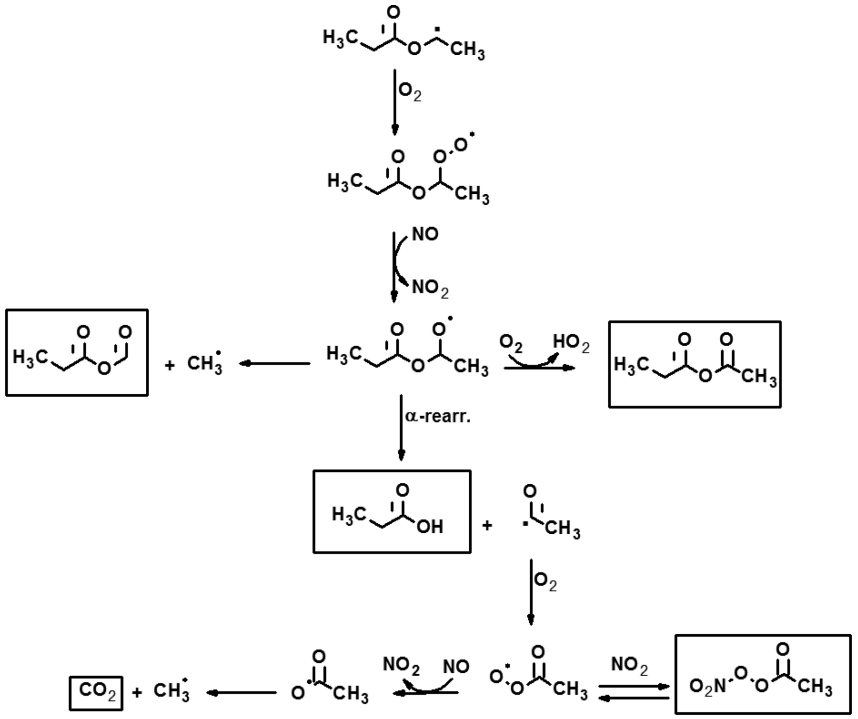

[a]Boxes indicate non-radical products.

Scheme 4. Suggested Reaction Mechanism for the Radical Produced by Reaction 1d[a]

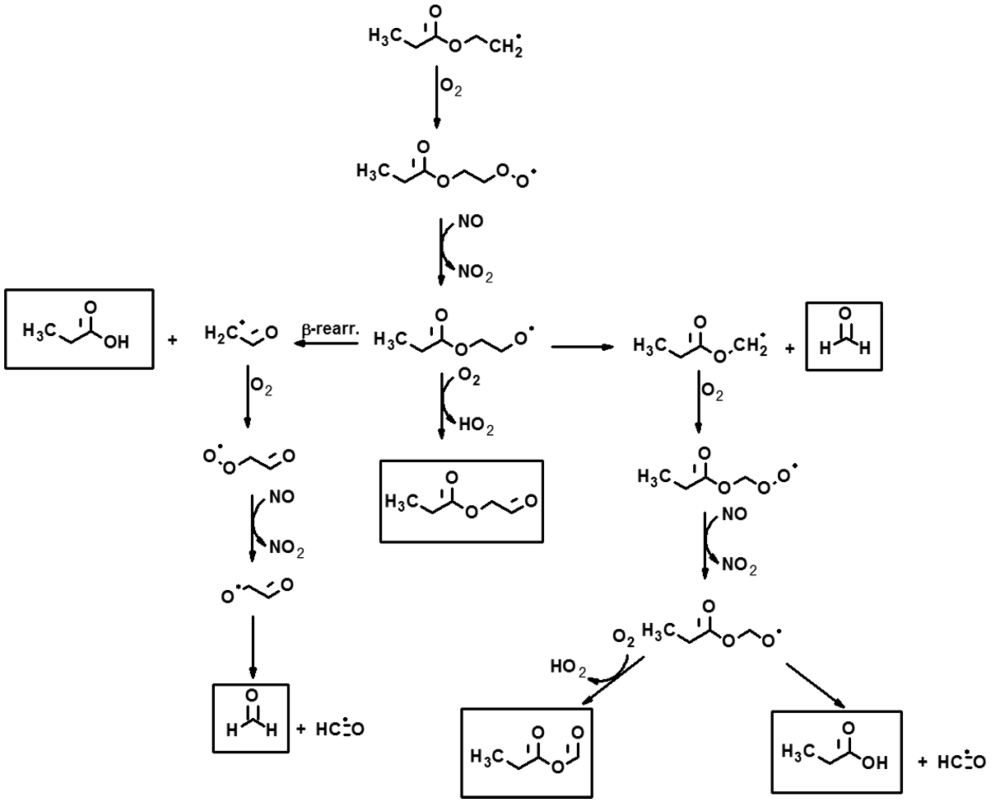

[a]Boxes indicate non-radical products.

observed for the structurally similar $CH_3CH(O)C(O)OCH_3$ alkoxy radical produced from oxidation of methyl propionate[13,28] for which decomposition producing acetaldehyde was observed. A possible explanation of this difference is the higher reactivity of the $-OCH_2-$ group of ethyl propionate compared to the $-OCH_3$ group of methyl propionate. The formation of a

dx.doi.org/10.1021/jp300897t | J. Phys. Chem. A 2012, 116, 5164−5179

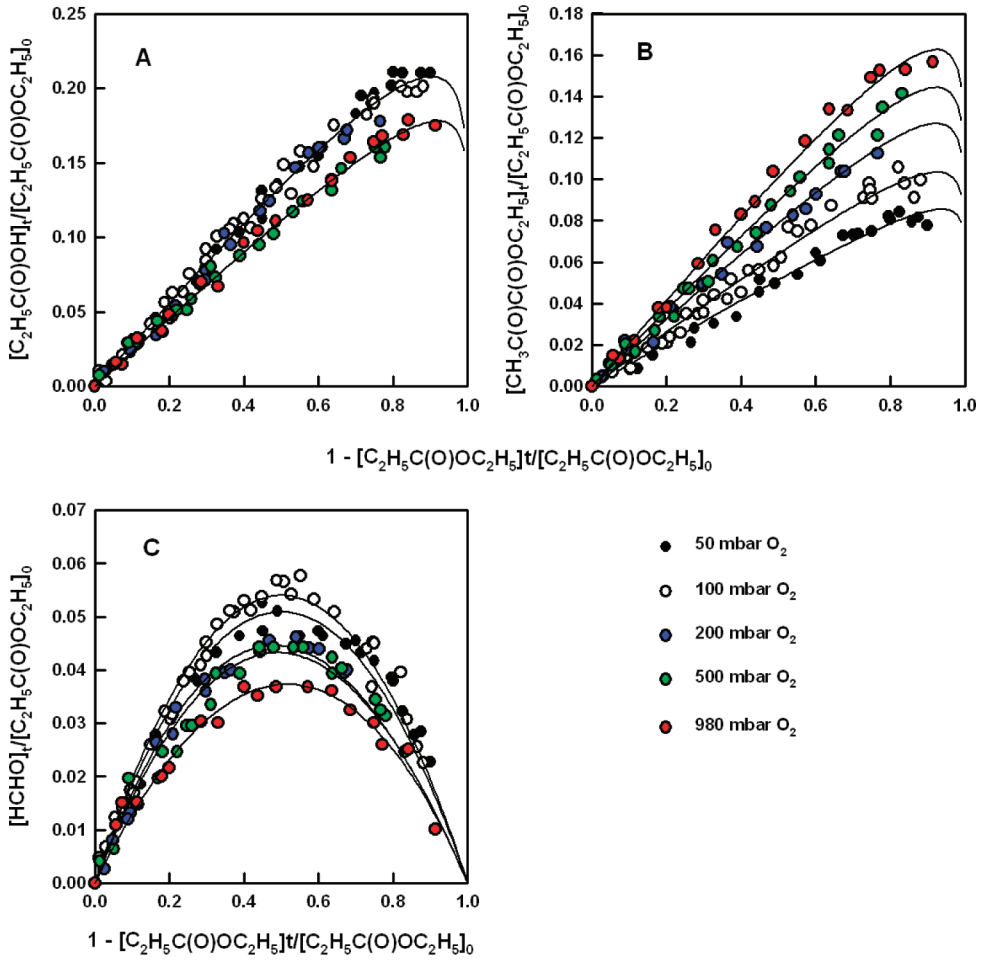

Figure 5. Formation of propionic acid (A), ethyl pyruvate (B), and formaldehyde (C) versus loss of ethyl propionate in 980 mbar total pressure of N_2 diluent with oxygen partial pressures of either 50 mbar (black), 100 mbar (white), 200 mbar (blue), 500 mbar (green), or 980 mbar (red).

relatively stable secondary radical in the case of ethyl propionate explains the higher tendency of the $CH_3CH(O)C(O)OC_2H_5$ to undergo isomerization rather than decomposition. Similar behavior has been observed for the structurally similar $(CH_3)(CH_2)CHC(O)OCH_3$ radical, which tends to undergo a hydrogen shift to produce the more stable tertiary $(CH_3)_2CC(O)OCH_3$ radical.[35]

The propionic acid observed in the spectra in Figure 4 can be generated by α-ester rearrangement of the secondary alkoxy radical formed by H-abstraction from the $-OCH_2-$ group of ethyl propionate (reaction 1c). The suggested reaction mechanism initiated by reaction 1c is shown in Scheme 3. The α-ester rearrangement is shown by reaction 23.

$$C_2H_5C(O)OCH(O)CH_3 \rightarrow C_2H_5COOH + C(O)CH_3 \quad (23)$$

Additional fates of the secondary alkoxy radical include reaction with oxygen to produce propionic acetic anhydride ($C_2H_5C(O)OC(O)CH_3$) (reaction 24) and decomposition to produce propionic formic anhydride ($C_2H_5C(O)OCHO$) and CH_3 (reaction 25).

$$C_2H_5C(O)OCH(O)CH_3 + O_2 \rightarrow C_2H_5C(O)OC(O)CH_3 + HO_2 \quad (24)$$

$$C_2H_5C(O)OCH(O)CH_3 \rightarrow C_2H_5C(O)OCHO + CH_3 \quad (25)$$

Neither propionic acetic anhydride nor propionic formic anhydride are commercially available, and their presence could not be confirmed with FTIR. Weak absorption peaks at 1050, 1145, 1300, and 1750 cm^{-1} are possibly due to propionic formic anhydride,[13] and absorption peaks in the frequency range 1760−1860 cm^{-1} are assigned to the C═O stretching vibrations of propionic acetic anhydride. GC-MS analysis also suggests the presence of this compound due to a chromatogram peak with a retention time of 10.7 min. The mass spectrum contains peaks at m/z = 43 and 57, which are assigned to $[C(O)CH_3]^+$ and $[C_2H_5C(O)]^+$ fragments, respectively.

The probable reaction mechanism initiated by reaction 1d is shown in Scheme 4. As for the other alkoxy radicals, the alkoxy radical generated by H-abstraction via channel 1d may react with O_2 (reaction 26), decompose (reaction 27), or rearrange (reaction 28).

$$C_2H_5C(O)OCH_2CH_2O + O_2 \rightarrow C_2H_5C(O)OCH_2CHO + HO_2 \quad (26)$$

$$C_2H_5C(O)OCH_2CH_2O \rightarrow C_2H_5C(O)OCH_2 + HCHO \quad (27)$$

dx.doi.org/10.1021/jp300897t | J. Phys. Chem. A 2012, 116, 5164−5179

$$C_2H_5C(O)OCH_2CH_2O \rightarrow C_2H_5C(O)OH + CH_2CHO \quad (28)$$

$C_2H_5C(O)OCH_2CHO$ is not commercially available and its presence, as well as reaction 26, could not be confirmed. Reaction 28 is a β-rearrangement occurring through a six-membered ring, and it provides an additional source of propionic acid. Propionic acid may also be formed by α-ester rearrangement of $C_2H_5C(O)OCH_2$. This radical is also produced in the oxidation of methyl proprionate, and it has been shown to undergo a competing reaction with oxygen to produce propionic formic anhydride.[13,28] In the present study it was not possible to distinguish between the different channels producing propionic acid. However, the results presented in section 6.1 suggest that the majority of the propionic acid comes from H-abstraction via channel 1c.

Formaldehyde, produced, for example, by reactions 16 and 27, is also observed in the spectra in Figure 4. Additional sources of formaldehyde include reaction of O_2 with CH_3 (reactions 29−31) produced in reaction 25, decomposition of $CH_2CH(O)O$ radicals (reaction 32) generated from CH_2CHO produced in reaction 28, or reaction of HO_2 with CHO (reaction 33) produced from either the α-rearrangement of $C_2H_5C(O)OCH_2$ or by reaction 32.

$$CH_3 + O_2 + M \rightarrow CH_3O_2 + M \quad (29)$$

$$CH_3O_2 + RO_2 \rightarrow CH_3O + RO + O_2 \quad (30)$$

$$CH_3O + O_2 \rightarrow HCHO + HO_2 \quad (31)$$

$$CH_2CH(O)O \rightarrow HCHO + CHO \quad (32)$$

$$CHO + HO_2 \rightarrow HCHO + O_2 \quad (33)$$

In Figure 5, the formation of the three products identified and quantified with FTIR are plotted versus the loss of ethyl propionate at the five different oxygen partial pressures used. In each case eq IV has been fitted to the data with product rate constants used in the fits provided in Table 4. The yields of a given experiment obtained from the fits is within the experimental error of the others and thus is not dependent on concentration. In general, the product rate constants derived from the fits are in good agreement with literature determinations (see Table 4). Product yields (determined by α in the fits) are provided in Table 5. The yield of propionic acid was slightly dependent on oxygen partial pressures with less of this compound being formed at high oxygen partial pressures (>500 mbar). The oxygen dependence reflects competing reactions such as reaction 23 and 24 or reactions 26 and 28. At oxygen partial pressures below 500 mbar, the molar yield of propionic acid was 0.283 ± 0.034, and at oxygen partial pressures of 500 mbar and above, the molar yield was 0.231 ± 0.029.

Table 4. Rate Constants for Reactions of Products Formed in the Cl-Initiated Oxidation of Ethyl Propionate

reaction	k (10^{-12} cm^3 molecule^{-1} s^{-1})	ref
$CH_3CHClC(O)OC_2H_5$	7.43 ± 0.78	this study[a]
$CH_3CHClC(O)OC_2H_5$	8.02 ± 3.04	this study[b]
$C_2H_5C(O)OH$ + Cl	3.27 ± 0.77	this study[b]
$C_2H_5C(O)OH$ + Cl	4.72 ± 0.62	Cavalli et al., 2000[28]
$CH_3C(O)C(O)OC_2H_5$ + Cl	2.63 ± 1.01	this study[b]
HCHO + Cl	56.4 ± 7.4	this study[b]
HCHO + Cl	71.1 ± 10.7	Atkinson et al., 2006[41]

[a]Determined with the relative rate method. [b]Derived from fits to the experimental data from the product studies. Errors represent weighted averages and an additional 10% experimental error.

The yield of ethyl pyruvate also showed an oxygen dependence with increasing ethyl pyruvate yields at increasing oxygen partial pressures. This oxygen dependence is evidence for a competing fate of the $CH_3CH(O)C(O)OC_2H_5$ radical, in this case the isomerization reaction 19. The maximum molar yield of ethyl pyruvate of 0.210 ± 0.054 in 980 mbar oxygen is in good agreement with the yield of ethyl-2-chloropropionate observed in 980 mbar N_2.

As seen from Table 4 and Figure 5, the yield of formaldehyde decreased with increasing pressure. This reflects the fact that formaldehyde is generally created via decomposition routes competing with oxygen reactions (see Schemes 1−4).

The competition between reaction with oxygen and decomposition or rearrangement reactions is in agreement with what has been observed for other oxygenated species, which are structurally similar to ethyl propionate, e.g., $C_2H_5C(O)OCH_3$,[13] $CH_3C(O)OC_2H_5$,[13] $(CH_3)_2CHC(O)OCH_3$,[35] $CH_3C(O)OCH_2CH_2OC_2H_5$,[36] and $C_2H_5OCH_2CH_2C(O)OC_2H_5$.[37]

The yields of the three products in the absence of NO correspond to a carbon balance of 31.5−38%.

6.3. Results in 980 mbar N_2/O_2 in the Presence of NO. In the presence of NO, the reaction mechanism of ethyl propionate was studied with oxygen partial pressures of 50, 200, 500, and 980 mbar in 980 mbar total pressure of N_2. Products observed in the absence of NO were also observed in the presence of NO in addition to nonidentified nitrated compounds and peroxyacetyl nitrate (PAN). PAN is produced by reactions 34 and 35 from the $CH_3C(O)$ radical generated in either reaction 21 or 23 (see Schemes 2 and 3).

$$CH_3C(O) + O_2 + M \rightarrow CH_3C(O)OO + M \quad (34)$$

$$CH_3C(O)OO + NO_2 + M \leftrightarrow CH_3C(O)OONO_2 + M \quad (35)$$

Reaction 35 is an equilibrium depending on the concentration of NO_2. The yield of PAN is also dependent on the NO_2/NO ratio, due to a competing reaction of the $CH_3C(O)OO$ peroxy radical with NO to produce CH_3 and CO_2 (reaction 36).

$$CH_3C(O)OO + NO \rightarrow CH_3 + CO_2 + NO_2 \quad (36)$$

The competition between reactions 35 and 36 is evident from the product plots in Figure 6F. The formation of propionic acid, formaldehyde, and ethyl pyruvate versus loss of ethyl propionate in the presence of NO is also plotted in Figure 6. For propionic acid and formaldehyde, results are shown at oxygen partial pressures of 50 and 980 mbar. The initial increase of all three products correlates linearly with the decrease in ethyl propionate. Fits of equations with the form of eq IV are shown by the dotted lines in the plots of propionic acid and formaldehyde (panels A−D). The rate constant ratios determined from these fits are not consistent with the product rate constants presented in Table 4, possibly due to interfering reactions with OH. In the presence of NO, OH radicals are generated by the reaction of NO with HO_2 produced from

dx.doi.org/10.1021/jp300897t | J. Phys. Chem. A 2012, 116, 5164−5179

Table 5. Product Yields in the Chlorine Atom Initiated Oxidation of Ethyl Propionate in 980 mbar Total Pressure of N_2 Diluent[a]

	O_2 partial pressure (mbar)					
product	0	50	100	200	500	980
	Molar Yields in % in the Absence of NO					
$ClCH_2CH_2C(O)OC_2H_5$	20.4 ± 3.1					
$CH_3CHClC(O)OC_2H_5$	25.1 ± 4.0					
$C_2H_5C(O)OCHClCH_3$	48.1 ± 8.8					
$CH_3C(O)C(O)OC_2H_5$		10.7 ± 2.7	13.3 ± 3.0	16.4 ± 4.1	18.6 ± 4.6	21.0 ± 5.4
C_2H_5COOH		27.9 ± 3.5	29.4 ± 3.8	27.9 ± 4.2	23.1 ± 3.2	23.6 ± 3.2
HCHO		20.4 ± 3.3	21.6 ± 2.9	18.9 ± 2.9	17.8 ± 3.1	14.2 ± 2.6
	Molar Yields in % in the Presence of NO					
$CH_3C(O)C(O)OC_2H_5$		7.7 ± 2.5		15.3 ± 4.4	14.5 ± 4.4	16.8 ± 3.9
C_2H_5COOH		39.6 ± 7.3		34.3 ± 6.6	27.4 ± 2.9	23.6 ± 3.0
PAN (80% $C_2H_5C(O)OC_2H_5$ consumption)		12.0 ± 1.2		34.6 ± 3.5	33.2 ± 3.3	24.7 ± 2.5
HCHO		7.9 ± 1.6		10.3 ± 2.4	13.7 ± 2.9	12.3 ± 3.5

[a]Quoted errors include 2 standard deviations of the fits of the data in Figures 3, 5 and 6 and 10% (20% for ethyl pyruvate) potential systematic uncertainty associated with the IR analysis.

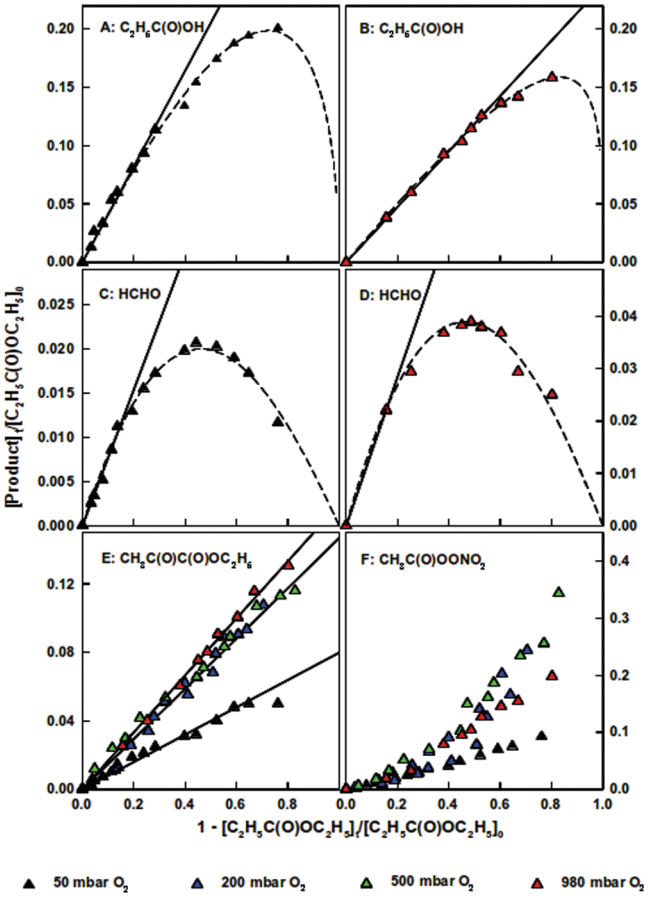

Figure 6. Formation of propionic acid (A,B), formaldehyde (C,D), ethyl pyruvate (E), and PAN (F) in the presence of NO. Black symbols: 50 mbar O_2; blue symbols: 200 mbar O_2; green symbols: 500 mbar O_2; red symbols: 980 mbar O_2. Dotted curves show fits to eq IV.

alkoxy radicals and oxygen (e.g., reactions 15 (Scheme 1), 17, 20 (Scheme 2), 24 (Scheme 3), and 26 (Scheme 4)).

$$NO + HO_2 \rightarrow NO_2 + OH \quad (37)$$

Due to this interference, the product yields are determined using the initial linearity of the product plots in Figure 6 (shown by solid lines). Results are shown in Table 5.

The yield of propionic acid decreased with increasing oxygen partial pressure, consistent with what was observed in the absence of NO. In general, the yields of propionic acid were higher in the presence of NO than in the corresponding experiments in the absence of NO. The effect was largest at low oxygen partial pressures. The higher yields of propionic acid in the presence of NO suggests that chemical activation of alkoxy radicals ($C_2H_5C(O)OCH(O)CH_3$, $C_2H_5C(O)OCH_2O$, or $C_2H_5C(O)OCH_2CH_2O$) is important. This phenomenon has been observed in several studies showing a higher yield of the α-ester rearrangement in the presence of NO_x.[13,28−30,33] An additional explanation of the higher yields of propionic acid in the presence of NO is the reaction with OH, which will change the product branching ratios. H-abstraction by OH from ethyl propionate is calculated to occur at the $-OCH_2-$ group 80% of the time (see section 7), which will be the main (if not the only) source of propionic acid.

The yields of ethyl pyruvate were slightly lower in the presence of NO. In contrast to what was observed in the absence of NO, there was only an oxygen effect at low oxygen partial pressures (<200 mbar). At oxygen partial pressures of 200−500 mbar, the molar yield of ethyl pyruvate was 0.149 ± 0.021. At 980 mbar it was 0.168 ± 0.039, and thus significantly lower than the yield of ethyl-2-chloropropionate obtained in 980 mbar N2. This shows that isomerization is more important in the presence of NO than in the absence of NO.

The yield of formaldehyde was generally lower in the presence of NO, except at oxygen partial pressures of 500−980 mbar, where there is no significant difference between experiments in the presence and absence of NO. In the presence of NO the yield of formaldehyde increased with increasing oxygen partial pressure, in contrast to what was observed in the absence of NO. The reason is not well understood but may involve OH reaction paths yielding formaldehyde.

The smaller yield of formaldehyde in the presence of NO at low oxygen partial pressure (≤200 mbar) relative to results in the absence of NO may be due to competition from reaction 35 (see Schemes 2 and 3) or 39 for the $C(O)OC_2H_5$ radical produced by the decomposition of $OCH_2C(O)OC_2H_5$ (see Scheme 1).

$$C(O)OC_2H_5 + O_2 \rightarrow OOC(O)OC_2H_5 \quad (38)$$

dx.doi.org/10.1021/jp300897t | J. Phys. Chem. A 2012, 116, 5164−5179

$$OOC(O)OC_2H_5 + NO_2 \rightarrow O_2NOOC(O)OC_2H_5 \quad (39)$$

$$OOC(O)OC_2H_5 + NO \rightarrow CO_2 + HCHO + CH_3 + NO_2 \quad (40)$$

In the absence of NO_x, reactions 36 and 40 will occur by reaction with RO_2 producing RO and O_2 in place of NO_2, and this will be the only fate of the peroxy radicals. In the presence of NO_x, reactions 35 and 39 will compete for peroxy radicals, leading to formaldehyde.

The product yields in Table 5 in the presence of NO correspond to a carbon balance of 37.8−51.8%. From the product yields given in Table 5, we conclude that H-abstraction by Cl from ethyl propionate occurs 20.4 ± 3.1% by reaction 1a, 25.1 ± 4.0% by reaction 1b, and 48.1 ± 8.8% by reaction 1c. The expected branching ratio of H-abstraction from the $-CH_3$ group (reaction 1d) is thus 0.064 ± 0.101. The results show that there is no significant difference between the reactivity of the alkoxy and the acyl end of ethyl propionate toward H-abstraction by Cl atoms.

7. RESULTS OF COMPUTATIONAL STUDIES

The mechanism for hydrogen abstraction from methyl ethyl propionate by the hydroxyl radical was investigated theoretically. Hydrogen abstraction can be divided into in-plane and out-of-plane reactions. We only consider the out-of-plane hydrogen atom on the two methyl groups ($-CH_3$). The in-plane hydrogen atom is less inclined to abstraction than the out-of-plane.[19] Reaction paths **1** and **2** are H-abstraction from CH_3- and $-CH_2-$ on the ethyl group (CH_3CH_2-), respectively, whereas reaction paths **3** and **4** are H-abstraction from $-CH_2-$ and $-CH_3$ on the ethoxy group ($-OCH_2CH_3$):

$$CH_3CH_2C(O)OCH_2CH_3 + OH \rightarrow CH_2CH_2C(O)OCH_2CH_3 + H_2O \quad \text{(reaction path 1)}$$

$$\rightarrow CH_3CHC(O)OCH_2CH_3 + H_2O \quad \text{(reaction path 2)}$$

$$\rightarrow CH_3CH_2C(O)OCHCH_3 + H_2O \quad \text{(reaction path 3)}$$

$$\rightarrow CH_3CH_2C(O)OCH_2CH_2 + H_2O \quad \text{(reaction path 4)}$$

The reaction products $CH_2CH_2C(O)OCH_2CH_3$, $CH_3CHC(O)OCH_2CH_3$, $CH_3CH_2C(O)OCHCH_3$, and $CH_3CH_2C(O)OCH_2CH_2$ are denoted as P1, P2, P3, and P4, respectively. The OH initated reaction are similar to Cl atoms initiated oxidation described by reactions 1a−1d.

All the geometries of the reactants, reactant complexes (RC), transition state structures (TS), product complexes (PC) and products are optimized at the BH&HLYP/aug-cc-pVTZ level of theory. Details for the optimized geometries and transition state energies are provided in the Supporting Information. The energy profile for the reaction between ethyl propionate and hydroxyl radical is shown for the four reaction paths in Figure 7.

The reactant complexes are shown in Figure 8. In the two reactant complexes, RC1 and RC3, ethyl propionate and the hydroxyl radical form a ring structure stabilized with two hydrogen bonds. There is a short H-bond between the hydrogen atom of the OH radical and the carbonyl group (>C═O) and two longer H-bonds between the oxygen atom in the OH group and the two out-of-plane hydrogen atoms. The reactant complexes RC2 and RC4 are identical; they have

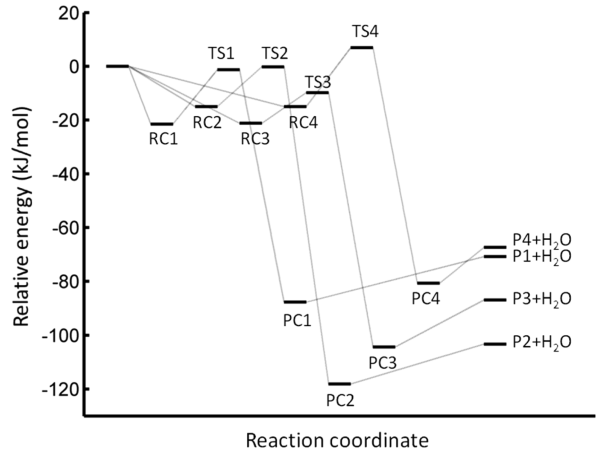

Figure 7. Energy profiles for the reaction between ethyl propionate and the hydroxyl radical for the four reaction reaction pathways. The products, P1, P2, P3, and P4, are $CH_2CH_2C(O)OCH_2CH_3$, $CH_3CHC(O)OCH_2CH_3$, $CH_3CH_2C(O)OCHCH_3$ and $CH_3CH_2C(O)OCH_2CH_2$, respectively. The symbols RC, TS, and PC denote the reactant complex, transition state, and product complexes along the reaction pathways. The level of theory is the CCSD(T)-F12a/VDZ-F12//BH&HLYP/aug-cc-pVTZ level of theory and the energy includes the ZPE.

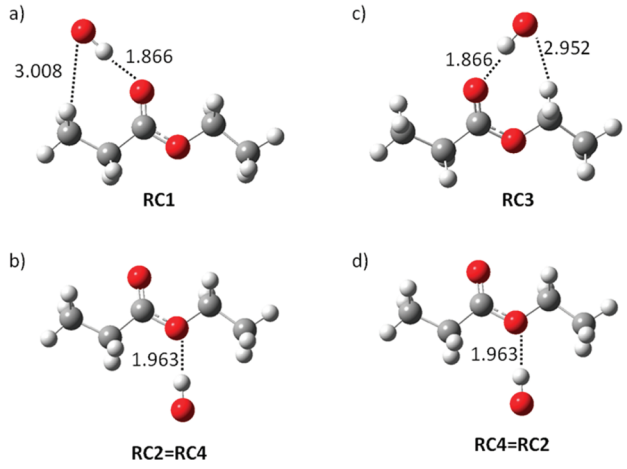

Figure 8. Reactant complexes are shown for the reaction between the OH radical and ethyl propionate. The reactant complexes are shown for the reaction paths (a) $CH_3CH_2C(O)OCH_2CH_3 + OH \rightarrow CH_2CH_2C(O)OCH_2CH_3 + H_2O$, (b) $CH_3CH_2C(O)OCH_2CH_3 + OH \rightarrow CH_3CHC(O)OCH_2CH_3 + H_2O$, (c) $CH_3CH_2C(O)OCH_2CH_3 + OH \rightarrow CH_3CH_2C(O)OCHCH_2 + H_2O$, and (d) $CH_3CH_2C(O)OCH_2CH_3 + OH \rightarrow CH_3CH_2C(O)OCH_2CH_2 + H_2O$. The geometries are optimized at the BH&HLYP/aug-cc-pVTZ level of theory. Distances are given in angstroms.

an open structure with only one hydrogen bond between the oxygen atom in the ether linkage (e.g., −O−) and the hydrogen atom in the OH radical. The reactant complexes with a ring structure, RC1 and RC3, are better stabilized than reactant complexes with an open structure like RC2 (RC4). The difference in stabilization energy is roughly 6 kJ/mol (see Figure 7).

The transition state structure for the reaction channels are shown in Figure 9. As for the reactant complexes, the transition states with a ring structure such as TS1 and TS3 are better stabilized than the ones with an open structure like TS2 and TS4. The transition state structure TS3 describing hydrogen

dx.doi.org/10.1021/jp300897t | J. Phys. Chem. A 2012, 116, 5164−5179

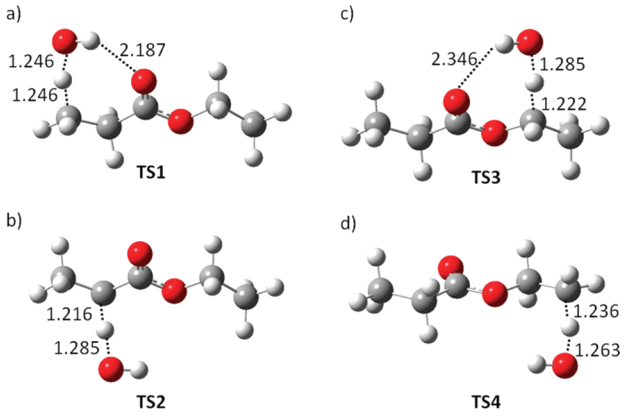

Figure 9. Transition state structures are shown for the reaction between the OH radical and ethyl propionate. The transition state structures are shown for the reaction paths (a) $CH_3CH_2C(O)OCH_2CH_3 + OH \rightarrow CH_2CH_2C(O)OCH_2CH_3 + H_2O$, (b) $CH_3CH_2C(O)OCH_2CH_3 + OH \rightarrow CH_3CHC(O)OCH_2CH_3 + H_2O$, (c) $CH_3CH_2C(O)OCH_2CH_3 + OH \rightarrow CH_3CH_2C(O)OCHCH_2 + H_2O$, and (d) $CH_3CH_2C(O)OCH_2CH_3 + OH \rightarrow CH_3CH_2C(O)OCH_2CH_2 + H_2O$. The geometries are optimized at the BH&HLYP/aug-cc-pVTZ level of theory. Distances are given in angstroms.

abstraction from $-OCH_2-$ is more reactant-like than transition state TS1 describing the hydrogen from the methyl group on the $C(O)CH_2CH_3$ fragment. Therefore, the lowest reaction barrier is observed for the hydrogen abstraction from $-OCH_2-$. This favors H-abstraction from $-OCH_2-$.

We have estimated the rates of H-abstraction for each of the hydrogen atoms. The total rate is the sum of the individual rate constants estimated at 298 K and 1 atm, and they are given in Table 6. We observe that the quantum tunneling effects vary; tunneling is 2−3 times greater for H-abstraction from the $-CH_3$ group than from the $-CH_2$ group. The total rate constant for OH oxidation is estimated to be 6.76×10^{-11} cm^3 molecule^{-1} s^{-1}. We overestimate the rate constant for ethyl propionate (see Table 1). The branching ratio (Γ) is the ratio between the individual rates and the total rate. We predict that approximately 80% of the reaction occurs at the $-OCH_2-$ group.

The rate constant and branching ratio are very sensitive to the stabilization energy of the reaction complexes (step 1) and the energy difference between the transition state and reactant complex (step 2). We expect that the accuracy of these energies is approximately 4 kJ/mol. If the energy of transition state TS3 is overestimated by 4 kJ/mol, then the rate constant for the second step will be reduced by approximately a factor of 0.2, leading to a branching of 50% in the reaction channel $CH_3CH_2C(O)OCHCH_3 + H_2O$. If the energy of the transition state TS2 is underestimated by 4 kJ/mol, then the rate constant will increase by a factor of 5, and the branching ratio in the reaction channel $CH_3CH_2C(O)OCHCH_3 + H_2O$ is 72%.

The present results can be compared with results obtained using the EPA's AOPWin structure reactivity method.[26] These calculations say that the reaction of ethyl propionate with OH will occur 8% via reaction path 1, 14% via reaction path 2, 70% via reaction path 3, and 8% via reaction path 4. As can be seen in Table 6, the branching ratio results largely agree.

8. IMPLICATIONS FOR ATMOSPHERIC CHEMISTRY

We report the first study of the Cl-initiated oxidation of ethyl propionate. The kinetic result for the reaction of ethyl propionate with OH is consistent with previously determined results. The rate constant for the reaction of ethyl propionate with Cl has been determined previously by one group, and the rate constants determined in the two studies are significantly different. Further research to clarify this discrepancy is needed. The negative activation energy for the Cl-initiated oxidation of ethyl propionate determined in the present study is confirmed by previous studies of other esters, and it suggests the formation of a prereaction complex.

From the rate constant determined for the reaction of ethyl propionate with OH combined with a global average OH concentration of 1×10^6 cm^{-3},[7] a lifetime of approximately 5 days for ethyl propionate is determined. This relatively long lifetime suggests that long-range transport of ethyl propionate will be important and that ethyl propionate will contribute inefficiently to local air quality impacts. This is supported by the estimated photochemical ozone creation potential (POCP) of ethyl propionate, 19.9,[38] which is lower than the POCP values of 27.1−41.1 for the most abundant compounds in diesel.[37] The products formed from ethyl propionate oxidation include carboxylic acids, anhydrides, keto-esters and aldehydes. These products tend to be less reactive than the parent ester, and the most probable fates include long-range transport, wet and dry deposition, and hydrolysis (in the case of anhydrides). An exception is formaldehyde, which reacts faster with atmospheric oxidants than ethyl propionate. The molar yields of formaldehyde are 8−20%, which is larger than is typical for the long-chain hydrocarbons present in standard diesel.

The present study shows that the alkoxy end of ethyl acetate is more reactive toward chlorine atoms relative to the acyl end. The main site of reaction for chlorine atoms and hydroxyl radicals is the $-OCH_2-$ group. A similar result has been obtained for ethyl acetate,[13] but in the case of ethyl acetate, no reaction with Cl was observed at the acyl end of the molecule.

Table 6. Equilibrium Constant K_{eq} (cm^3 molecule^{-1}) of the First Step, the Rate Constant k_2 (s^{-1}) of the Second Step, the Eckart Tunnelling Correction κ (Dimensionless), the Total Reaction Rate Constant k (cm^3 molecule^{-1} s^{-1}) for the Overall Reaction, and the Branching Ratio Γ (%)[a]

	K_{eq}	k_2	κ	k	Γ (a)	Γ (b)
$CH_3CH_2C(O)OCH_2CH_3 + OH \rightarrow CH_2CH_2C(O)OCH_2CH_3 + H_2O$	1.5×10^{-21}	2.8×10^8	20	8.2×10^{-12}	12	8
$CH_3CH_2C(O)OCH_2CH_3 + OH \rightarrow CH_3CHC(O)OCH_2CH_3 + H_2O$	2.3×10^{-22}	2.0×10^9	7	3.4×10^{-12}	5	14
$CH_3CH_2C(O)OCH_2CH_3 + OH \rightarrow CH_3CH_2C(O)OCHCH_3 + H_2O$	1.2×10^{-21}	7.1×10^9	6	5.4×10^{-11}	80	70
$CH_3CH_2C(O)OCH_2CH_3 + OH \rightarrow CH_3CH_2C(O)OCH_2CH_2 + H_2O$	2.3×10^{-22}	4.4×10^8	16	1.7×10^{-12}	3	8

[a] (a) Estimated at CCSD(T)-F12a/VDZ-F12//BH&HLYP/aug-cc-pVTZ level of theory. The results are given at 298 K. (b) Branching ratios calculated with EPA's AOPWin structure reactivity method.

dx.doi.org/10.1021/jp300897t | J. Phys. Chem. A 2012, 116, 5164−5179

Compared to the acetates, the presence of a $-CH_2$ group on the acyl end of the molecule increases the reactivity of this part of the molecule. This was also seen in a previous study of methyl propionate.[13]

The plant oils used for making biodiesel typically contain long chain fatty acids (e.g., palmitic acids, $CH_3(CH_2)_{14}C(O)$-OH, and stearic acid, $CH_3(CH_2)_{16}C(O)OH$), and the reactivities of the ethyl esters of such compounds are expected to approach that of the corresponding alkanes. The mechanism for reaction at the carbon groups close to the ester functionality is expected to be similar to what is observed in the present study, whereas reaction of carbon groups further away from the ester functionality will result in products that resemble those from the oxidation of the corresponding alkanes. Comparison of the present results for ethyl propionate with results obtained for methyl propionate in a previous study[13] suggests that reaction of the alkoxy end of the molecule will be larger for ethyl esters than for methyl esters, and the ester functionality is therefore expected to excercise a larger influence on FAEEs than on FAMEs. Further studies of the atmospheric chemistry of larger esters more representative of biodiesel would be helpful to provide a better understanding of the atmospheric fate of such molecules.

■ ASSOCIATED CONTENT

Supporting Information

Table S1: Electronic energies and zero point vibration energies. Table S2. Cartesian coordinates of the mentioned structures. Figure S1: Structures of the product complexes. Figure S2: The structure of ethyl propionate and the structure of the four product radicals. This material is available free of charge via the Internet at http://pubs.acs.org.

■ AUTHOR INFORMATION

Corresponding Author

*E-mail: msj@kiku.dk.

Notes

The authors declare no competing financial interest.

■ ACKNOWLEDGMENTS

The authors thank the Copenhagen Center for Atmospheric Research, sponsored by the Danish Natural Science Research Council, the Villum Kann Rasmussen Fund, and EUROCHAMP2 for their generous support. We thank the Danish Center for Scientific Computing (DCSC) for computational support.

■ REFERENCES

(1) Anderson, J. E.; Baker, R. E.; Hardigan, P. J. ; Ginder, J. M. ; Wallington, T. J. *Society of Automotive Engineers Technical Paper* 2009, 09FFL-0302

(2) Directive 2009/28/EC of The European Parliament and of the Council, 2009, Official Journal of the European Union, L 140/16.

(3) Bendtz, K. *EU-25 - Oilseeds and Products: Biofuels Situation in the European Union 2005*, GAIN Report; USDA and Foreign Agricultural Service: Washington DC, 2007.

(4) Wang, P. S.; Thompson, J.; Clemente, T. E.; Van Gerpen, J. H. *Trans. ASABE* **2010**, *53*, 1853.

(5) Baiju, B.; Naik, M. K.; Das, L. M. *Renewable Energy* **2009**, *34*, 1616.

(6) Demirbas, A. *Appl. Energy* **2009**, *86*, 108.

(7) Prinn, R.; Weiss, R. R.; Miller, B. R.; Huang, J.; Alyea, F. N.; Cunnold, D. M.; Fraser, P. J.; Hartley, D. E.; Simmonds, P. G. *Science* **1995**, *269*, 187.

(8) Finlayson-Pitts, B.; Pitts, J. R. *Chemistry of the Upper and Lower Atmosphere*; Academic Press: San Diego, CA, 2000.

(9) Raff, J. D.; Njegic, B.; Chang, W. L.; Gordon, M. S.; Dabdub, D.; Gerber, B.; Finlayson-Pitts, B. J. *Proc. Natl. Acad. Sci. U.S.A.* **2009**, *106*, 13647.

(10) Spicer, C. W.; Chapman, E. G.; Finlayson-Pitts, B. J.; Plastridge, R. A.; Hubbe, J. M.; Fast, J. D.; Berkowitz, C. M. *Nature* **1998**, *394*, 353.

(11) Mellouki, A.; Le Bras, G.; Sidebottom, H. *Chem. Rev.* **2003**, *103*, 5077.

(12) Calvert, J. G.; Mellouki, A.; Orlando, J. J.; Pilling, M. J.; Wallington, T. J. *Mechanisms of Atmospheric Oxidation of the Oxygenates*; Oxford University Press: New York, 2011.

(13) Andersen, V. F.; Bernhanu, T. A.; Nilsson, E. J.; Jørgensen, S.; Nielsen, O. J.; Wallington, T. J.; Johnson, M. S. *J. Phys. Chem. A* **2011**, *115*, 8906.

(14) Cometto, P. M.; Daële, V.; Idir, M.; Lane, S. I.; Mellouki, A. *J. Phys. Chem. A.* **2009**, *113*, 10745.

(15) Wallington, T. J.; Dagaut, P.; Liu, R.; Kurylo, M. J. *Int. J. Chem. Kinet.* **1988**, *20*, 177.

(16) Nilsson, E. J.; Eskebjerg, C.; Johnson, M. S. *Atmos. Environ.* **2009**, *43*, 3029.

(17) Lee, C. T.; Yang, W. T.; Parr, R. G. *Phys. Rev. B* **1998**, *37*, 785−789.

(18) Becke, A. D. *J. Chem. Phys.* **1993**, *98*, 1372−1377.

(19) Dunning, T. H. *J. Chem. Phys.* **1989**, *90*, 1007−1023.

(20) Frisch, M. J. et al. *Gaussian 03*, revision C.02; Gaussian, Inc.: Wallingford, CT, 2004.

(21) Adler, T. B; Knizia, G.; Werner, H. J. *J. Chem. Phys.* **2007**, *127*, 221106.

(22) Peterson, K. A; Adler, T. B.; Werner, H. J. *J. Chem. Phys.* **2008**, *128*, 084102.

(23) Werner, H.-J.; Knowles, P. J.; Lindh, R.; Manby, F. R.; Schutz, M.; Celani, P.; Korona, T.; Rauhut, G.; Amos, R. D.; Bernhardsson, A.; Berning, A.; Cooper, D. L.; Deegan, M. J. O.; Dobbyn, A. J.; Eckert, F. ; Hampel, C. ; Hetzer, G.; Lloyd, A. W.; McNicholas, S. J.; Meyer, W.; Mura, M. E.; Nicklass, A.; Palmieri, P.; Pitzer, R., Schumann, U.; Stoll, H.; Stone, A. J.; Tarroni, R.; Thorsteinsson, T.; *MOLPRO*, version 2010.1, see http://www.molpro.net.

(24) Eckart, C *Phys. Rev.* **1930**, *35*, 1303−1309.

(25) Cuevas, C. A.; Notario, A.; Martínez, E.; Albadaladejo, J. *Atmos. Environ.* **2005**, *39*, 5091.

(26) U.S. EPA. EPI Suite AOPWin, v 1.92.

(27) Meagher, R. J.; McIntosh, M. E.; Hurley, M. D.; Wallington, T. J. *Int. J. Chem. Kinet.* **1997**, *29*, 619.

(28) Cavalli, F.; Barnes, I.; Becker, K. H.; Wallington, T. J. *J. Phys. Chem. A* **2000**, *104*, 11310.

(29) Christensen, l. K.; Ball, J. C.; Wallington, T. J. *J. Phys. Chem.* **2000**, *104*, 345.

(30) Tyndall, G. S.; Pimentel, A. S.; Orlando, J. J. *J. Phys. Chem. A* **2004**, *108*, 6859.

(31) Tuazon, E. C.; Aschmann, S. M.; Atkinson, R.; Carter, W. P. L. *J. Phys. Chem. A* **1998**, *102*, 2316.

(32) Picquet-Varrault, B.; Doussin, J.-F.; Durand-Jolibois, R.; Carlier, P. *Phys. Chem. Chem. Phys.* **2001**, *3*, 2595.

(33) Andersen, V. F.; Nilsson, E. J. K.; Jørgensen, S.; Nielsen, O. J.; Johnson, M. S. *Chem. Phys. Lett.* **2009**, *472*, 23.

(34) Orlando, J. J.; Tyndall, G. S. *Int. J. Chem. Kinet.* **2010**, *42*, 397.

(35) Wyatt, S. E.; Baxley, J. S.; Wells, R. *Int. J. Chem. Kinet.* **1999**, *31*, 551.

(36) Wells, J. R.; Wiseman, F. L. *Int. J. Chem. Kinet.* **1996**, *28*, 475.

(37) Baxley, J. S.; Henlsy, M. V.; Wells, J. R. *Int. J. Chem. Kinet.* **1997**, *29*, 637.

(38) Jenkin, M. E.; Passant, N. R.; Rudd, H. J.*Development of Species Profiles for UK Emissions of VOCs*; Report AEAT\EPSC-0044, Issue 1; AEA Technology: Abingdon, U.K., 2000

(39) Wine, P. H.; Semmes, D. H. *J. Phys. Chem.* **1983**, *87*, 3572.

(40) Wallington, T. J.; Andino, J. M.; Lorkovic, I. M.; Kaiser, E. W.; Marston, G. J. *J. Phys. Chem.* **1990**, *94*, 3644.

(41) Atkinson, R.; Baulch, D. L.; Cox, R. A.; Crowley, J. N.; Hampson, R. F.; Hynes, R. G.; Jenkin, M. E.; Rossi, M. J.; Troe. *J. Atm. Chem. Phys.* **2006**, *6*, 3625.
(42) Calvert, J. G.; Derwent, R. G.; Orlando, J. J.; Tyndall, G. S.; Wallington, T. J. *Mechanisms of Atmospheric Oxidation of the Alkanes*; Oxford University Press: New York, 2008.